Available online at www.sciencedirect.com

ScienceDirect

Energy Procedia 69 (2015) 1810 – 1818

Energy Procedia

International Conference on Concentrating Solar Power and Chemical Energy Systems, SolarPACES 2014

Heat transfer simulation in a high temperature solar reactor

P. Parthasarathy[a], P. Le Clercq[a]

[a]*Deutsches Zentrum für Luft- und Raumfahrt (DLR), Pfaffenwaldring 38-40, 70569 Stuttgart, Germany.*

Abstract

The fluid flow coupled to radiative, convective and, conductive heat transfer is computed within a solar reactor containing a reticulated porous ceramics (RPC) domain made out of ceria (cerium dioxide, CeO_2). A Monte-Carlo radiation model is used in the fluid regions of the reactor with source terms outside the cavity's window to account for the concentrated radiative power input. Darcy's law for the viscous regime and the Forchheimer's term for the inertial regime are used in the momentum equation to account for the pressure drop within the porous region (RPC). Two separate energy equations for the solid and for the fluid regions of the porous domain are solved in order to capture the non-equilibrium effects in that region. Rosseland's diffusion approximation is used in the solid regions of the RPC domain. The material properties and boundary conditions were taken from published experimental measurements. The simulation results are compared to the measurement data collected during the pre-heating and the ceria reduction phases, which sum up to four different radiative power inputs. Results of the comparison are good and constitute the verification that the numerical methods, physical sub-process models and material properties are adequately selected and implemented.

Peer review by the scientific conference committee of SolarPACES 2014 under responsibility of PSE AG

Keywords: Monte-Carlo radiation model; Darcy-Forchheimer equation; Rosseland approximation.

1. Introduction

The effective conversion of CO_2 and H_2O into a transportable and storable chemical fuel with high energy density using abundantly available solar energy has been a path breaking field of study in recent years [1,2,3,4,5]. With the use of solar cavity-receiver reactors, the generation of syngas (H_2 and CO) out of CO_2 and H_2O through a solar-driven thermochemical cycle based on metal oxide redox reactions are made more efficient and stable [1,2]. This syngas may enable large scale liquid hydrocarbon fuel production using the industrially mature Fischer–Tropsch (F-

Peer review by the scientific conference committee of SolarPACES 2014 under responsibility of PSE AG
doi:10.1016/j.egypro.2015.03.154

T) process. Furthermore, F-T synthetic paraffinic kerosene is an ASTM International approved blend stock for aviation turbine fuels. The two-step thermochemical cycle using metal oxide redox reactions are reported to be more practical and efficient in comparison to the direct thermolysis of H_2O [8,20]. Among the various redox materials e.g. ZnO, SnO_2, ferrous based metal oxides, ceria (CeO_2) is considered to be a more suitable material for syngas production [1], and among various structures of metal oxides that are studied, e.g. monolithic pins, honey combs, felts, ordered porous structures, lattice structures, ceria in the form of a reticulated porous ceramic (RPC) structure has demonstrated so far the highest solar-to-fuel energy conversion efficiency [2]. The performance of a solar reactor in converting solar energy into syngas is expressed in terms of solar-to-fuel energy conversion efficiency [1,2,6], which is defined as [1,2]

$$\eta_{solar-fuel} = \frac{\Delta H_{fuel} r_{fuel}}{P_{solar} + E_{penalties}} \tag{1}$$

where ΔH_{fuel} is the high heating value of the fuel, P_{solar} is the radiative power input, r_{fuel} is the total amount of fuel produced and $E_{penalties}$ is the system specific energy penalties such as consumption of inert gas, electricity, or pumping work.

A thermodynamic analysis of the solar cavity-receiver numerically investigated here shows that the solar-to-fuel energy conversion efficiency without heat recovery can be up to 20% and can reach 30% with 50% heat recovery [6]. In practice, solar thermochemical splitting of CO_2 reached an average $\eta_{solar\text{-}fuel}$ of 1.73% (Furler *et al*. [2]), which is four times higher than the next best reported value for a solar-driven device. Out of the total solar power input, the re-radiated power, and the power required in heating inert gas and the power loss from the reactor surface to the surrounding contributes to the conductive, radiative and convective losses in the reactor. Along with the experimental results that are available in the literature regarding the efficiency and the heat transfer in the porous reactor, further numerical simulations of the heat transport and the subsequent thermochemical reactions will help selecting the favorable RPC structure with optimal structural properties (e.g., porosity, specific area, etc.), and also will facilitate in further optimizing the reactor design. The overall modeling strategy and numerical method presented here should enable future design and heat balance optimization in order to approach the reported theoretical energy conversion efficiency. In this paper, the heat transport through a compound parabolic concentrator (CPC) and within the solar cavity-receiver containing reticulated porous ceramics (RPC) made of pure CeO_2 is numerically verified by comparing computation results with the experimental data of Furler *et al.* [2].

Nomenclature

A	area
c_F	drag constant
c_{pf}	specific heat capacity of fluid at constant pressure
c_{ps}	specific heat capacity of solid at constant pressure
H	enthalpy
h	heat transfer coefficient
K	permeability
k_f	conductivity of fluid
k_s	conductivity of solid
n	refractive index
P	power
p	pressure
Q_{fs}	convective heat source from fluid to solid
Q_{sf}	convective heat source from solid to fluid
Q_r	radiative heat source
q_r	radiative heat flux

T_f	temperature of fluid
T_s	temperature of solid
t	time
u_s	superficial velocity
u	velocity
α	absorption coefficient
β	extinction coefficient
ε	porosity
η	efficiency
μ	dynamic viscosity
ρ_f	density of fluid
ρ_s	density of solid
σ	Stefan Boltzmann constant
τ	optical thickness
ϵ	emissivity

2. Solar reactor configuration

A detailed description of the solar reactor design, its dimensions and, its integration in an experimental setup are described in details in [1,2,7]. The measurements, which are used here as benchmark, were performed at the ETH Zurich, Department of Mechanical and Process Engineering. A short summary of the solar reactor configuration is provided hereafter. The external thermal radiation closely resembling the characteristics of a concentrating solar power (CSP) system was provided by a high-flux solar simulator (HFSS); an array of Xe-arc lamps which are closed coupled to truncated ellipsoidal reflectors. The radiation energy from the HFSS is concentrated onto the cavity-receiver. A compound parabolic concentrator (CPC) having an inlet aperture of 4 cm is attached to the exit of the cavity-receiver to further increase the concentration ratio and to reduce re-radiation losses. The reactor's aperture is sealed using a 24 cm diameter and 3 mm thick fused quartz window. The cavity-receiver and CPC are water cooled and temperature was maintained at 300 K. The cavity-receiver of the solar reactor consists of a cylindrically shaped ceria RPC, which is exposed to the concentrated solar radiation. The cavity-receiver wall is made of Inconel 600 and has an inner Al_2O_3 thermal insulation. A thin wall of ceria laminate is placed in the annular space between the ceria RPC and the Al_2O_3 insulation. Argon gas was injected close to the aperture to cool down the window as well as into the annular gap between the ceria laminate and the RPC, through four radial inlet ports to purge the reactor. The product gases exits through an axial outlet port at the bottom of the receiver.

The ceria RPC is pre-heated to a temperature of around 1000 K using a solar power input of 0.8 kW, measured at the exit of the CPC. The pre-heating is followed by a reduction step. The two-step splitting of H_2O and CO_2 consist of a solar reduction step, in which the ceria RPC is heated above 1200 K to thermally reduce ceria [1,2]. The reduction step is followed by the oxidation step, which requires no solar power input. In the experiments, the oxygen yield and efficiency during reduction step is studied using three different solar power inputs of 2.8 kW, 3.4 kW and 3.8 kW [2]. The focus of the present numerical study is on the heat transfer during this reduction step.

3. Numerical methodology

In the present work, the simulations are carried out using the commercially available ANSYS CFX software. The computational volumes are of hexahedral structure and the resulting grid consisted of approximately 1.6 million hexahedral cells and approximately 1.7 million nodal points. ANSYS CFX employs the cell-centered finite volume method whereby flow variables being stored at the nodes. A second order interpolation scheme is used for the finite volume flux calculations. To capture the true transients in the reactor flow and heat transfer, unsteady computations using second order backward Euler scheme with adaptive time step (0.01 s - 0.5 s) is used. Newtonian fluids with variable density (accounting for buoyancy) are flowing within the domains. The flow boundary conditions at the inlet and outlet were specified using constant Argon gas velocity at inlet and static pressure together with zero

gradient condition for the velocity at the outlet. Volume averaged porous model is assumed in the RPC domain. Convective heat transfer is considered between the outer Inconel surface and the ambient air.

Numerical simulations are carried out to validate the models used to predict the heat transport and the fluid flow in the solar reactor. The simulations are performed with the fluid flow conditions as in the experiments [2] for four different solar power input settings at the CPC exit, i.e., P = 0.8kW, 2.8 kW, 3.4 kW and 3.8 kW. In the experiments the external source of thermal radiation (to replicate a highly concentrated solar power from a solar tower or dishes) was provided by a High-Flux Solar Simulator (HFSS) [1,2]. The focal point of the concentrated solar energy lies on the aperture of the compound parabolic concentrator. ANSYS CFX Monte-Carlo model does not have the possibility to specify the direction of each ray independently.

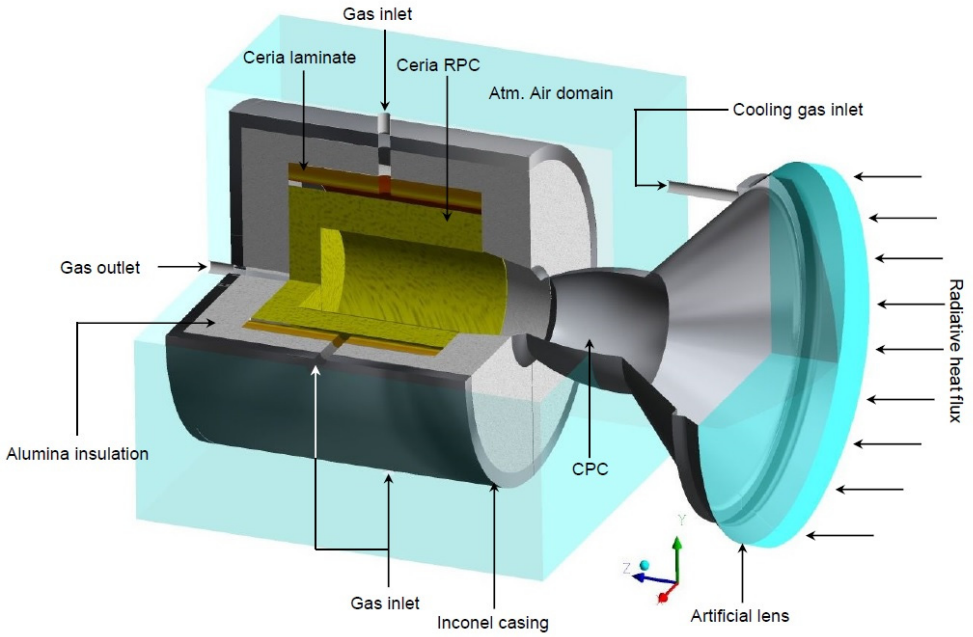

Fig. 1. The schematic cut-section of the solar reactor domain with the factitious lens domain.

In order to replicate the experimental conditions, a factitious (imaginary) plano-convex lens domain is included to the solar reactor domain. The lens domain is considered to be a fluid domain with air as the fluid medium, but the refractive index of the air in this domain is altered to a larger value in order to facilitate the focusing of the rays onto the CPC aperture. The schematic of the solar reactor domain with the artificial lens is shown in Fig. 1. According to the power required at the CPC exit, the input solar power is calculated using Eq. (2) [9] and the average transmission loss due to the presence of the artificial lens domain of high refractive index is calculated using Fresnel's equation and the input power is compensated for the transmission loss.

$$\eta_{abs} = \frac{\alpha_{eff} \cdot P_{aperature} - \in_{eff} \pi r^2 \sigma T^4}{P_{in}} \tag{2}$$

3.1. Flow through ceria RPC

A volume averaged porous model [10] is specified in the RPC domain. It is considered that the infinitesimal control volumes are relatively large in comparison to the interstitial spacing of the porous medium and are relatively

small with respect to the scales that have to be resolved [10,11]. Darcy's equation with added Forchheimer term Eq. (3) is used to account for momentum loss due to increased pressure drop within the porous region. In flows with pore Reynolds number greater than unity, the Forchheimer term becomes comparable to the surface drag due to friction [12]. The non-linear Forchheimer term is used to account for the form drag due to the solid structures. The porous regions are considered to be isotropic. The permeability *K*, the drag constant values of 10 and, a PPI 64% porosity ceria RPC are taken from [13].

$$\nabla p = -\frac{\mu}{K}\mathbf{u}_s - \frac{c_F}{\sqrt{K}}\rho_f \,|\,\mathbf{u_s}\,|\,\mathbf{u_s} \tag{3}$$

3.2. Radiation in fluid domain

A Monte-Carlo radiation model is used to model the radiative heat transfer. Large numbers of rays (10^7 in numbers) are traced for their incidence, reflection and absorption within the solar reactor. A uniform radiative heat flux is specified as boundary source at the lens upper surface. The rays are focused onto the CPC inlet aperture thanks to the difference in the refractive index between the lens medium and the outer air. The fluid (Ar) is considered to be gray, i.e., the radiative properties of the fluid are assumed to be independent of wavelength. The fluid media is considered to be a participating media and isotropic scattering is assumed. The walls of the cavity-receiver and of the CPC are considered to be opaque and specularly reflecting surfaces, and the emissivity of these polished aluminum surfaces is taken to be 0.1 [13]. All other wall surfaces (i.e., Al_2O_3 insulation, ceria laminate etc.) are assumed to be opaque and diffusely reflecting surfaces and their emissivity values are taken from [19]. Local fluid temperature boundary condition is employed at inlet and outlet boundaries.

3.3. Heat transfer in porous domain

In case of single phase fluid flow through porous matrix structures, the assumption of local thermal equilibrium is not valid in all engineering applications [15]. For porous media in solar reactor applications, there is a significant amount of radiative heat absorption in the solid phase, and the local solid and fluid volumes will not be in thermal equilibrium. When accompanied with an interstitial fluid flow within the porous matrix with significantly different thermal properties than that of the solid phase, the local change in temperature between the two phases will not be the same. In such applications, two energy equations are required in order to solve the heat transfer in the solid and in the fluid phases. A non-thermal equilibrium model is considered within the porous domain, given that the control cells and control surfaces are assumed to contain both solid and fluid regions. Separate energy equations for the solid region Eq. (4) and for the fluid region Eq. (5) are solved [16]. The solid-phase and the fluid-phase energy equations are coupled through convective heat transfer between the two phases and the use of an interfacial convective heat transfer coefficient Eq. (6).

$$\varepsilon\rho_f c_{pf}\frac{\partial T_f}{\partial t} + \left(\varepsilon\rho_f c_{pf}\right)\cdot u\cdot\nabla T_f = k_f\nabla\cdot\nabla T_f + Q_{fs} \tag{4}$$

$$(1-\varepsilon)\rho_s c_{ps}\frac{\partial T_s}{\partial t} = k_s\nabla\cdot\nabla T_s + Q_{sf} + Q_r \tag{5}$$

$$Q_{fs} = -Q_{sf} = h\cdot A\cdot(T_s - T_f) \tag{6}$$

3.3.1. Radiation in porous domain

The smallest dimension of the ceria RPC used in the experiment being L = 20 mm [2] and its extinction coefficient being κ = 500 mm^{-1} [13], the optical thickness τ of the porous rector is 10, i.e., ($\tau = \kappa \times L$), which is much greater than unity, and so, the porous region can be considered optically thick [15].The fluid regions within the porous domain are considered to be transparent, as their extinction coefficient is much less compared to that of the solid struts. As the region is optically thick, i.e., the mean free path for the radiation to travel is much less in comparison to the porous dimension, the radiation is considered as a diffusion process [18]. The diffusion form of radiative flux is given by the Rosseland equation Eq. (7). The divergence of the radiative flux is added as a source in the solid energy equation Eq. (5). Convective boundary condition is employed between the solid strut surfaces.

$$q_r = -\frac{16\sigma n^2 T_s^3}{3\beta}\nabla T_s \tag{7}$$

4. Results and discussion

In order to validate the models used for flow and heat transfer, simulations were performed for all four power inputs, corresponding to solar concentration ratios C between 636 suns and 3024 suns (solar concentration ratio C = P/(AI) is defined as the ratio of power intercepted by the CPC exit to the product of intercepting area and direct normal solar radiation I = 1kWm^{-2}[1,2,7]). The computations were performed using four 8-core processors with 32 GB RAM, requiring 120 hours of computation time for the pre-heating step and approximately 88 hours for the reduction step. From the simulations, the radiative flux distribution of the concentrated solar energy and its directional characteristics were obtained. The distribution of the solar radiative flux within the fluid domain is shown in Fig. 2. As expected, the concentrated flux distribution at the CPC aperture, i.e., at the focal point, has a typical bell shaped profile. The bell shaped profile which can be approximated as a Gaussian profile has a narrow peak, and the width of the narrow band is dependent on the coarseness of the grid, the higher the computational elements, the narrower and smoother the peak becomes. The narrow peak may represent a high quality concentrator (in experiments it may be difficult to realize very sharp focusing by the concentrators). In these simulations, as the Monte-Carlo algorithm using 10^7 particles is computationally intensive, the number of elements for the solar flux computations is 64 times less than the number of elements in the actual fluid mesh.

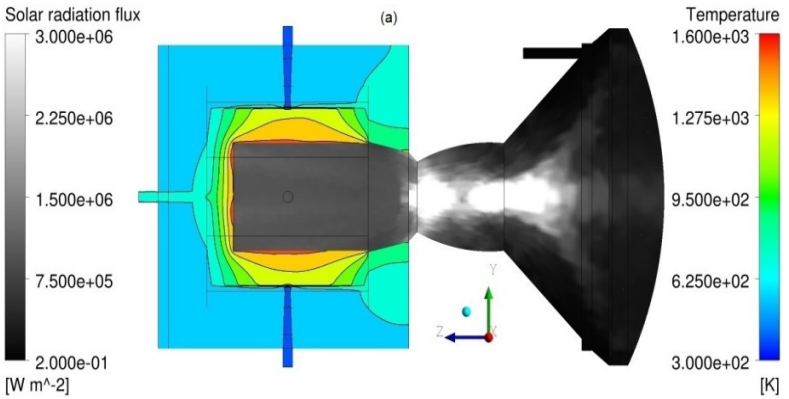

Fig. 2. (a) Cut-plane view showing the solar radiation flux distribution (grey-scale) and the temperature contours (color scale) inside the reactor for power input P = 0.8 kW; (b) Concentrated radial solar radiative flux distribution at CPC aperture.

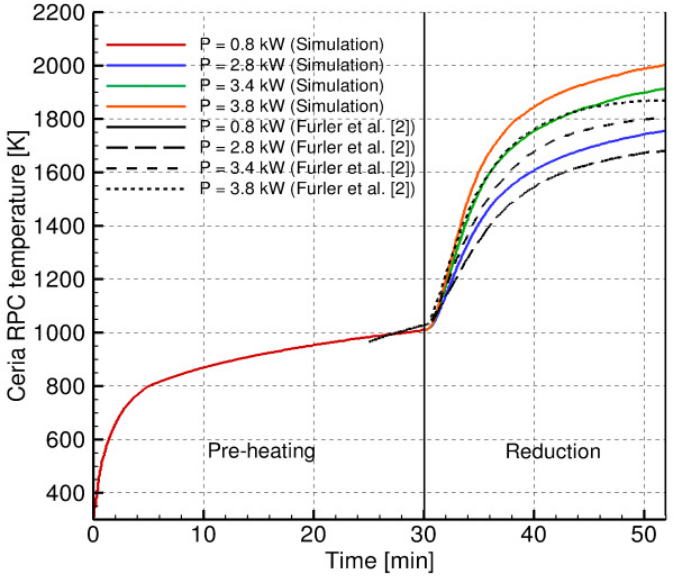

Fig. 3. Comparison of nominal reactor temperatures with experiments (simulations do not account for thermal reduction of ceria RPC).

At present, the thermochemical reduction of ceria is not included in the simulations, only the heat transport is calculated. Shown in Fig. 3 is the comparison of experimental and simulated temperature with respect to time. The computed temperature profiles are similar to that of the experiments with temperature values slightly higher. The reason can be attributed to the fact that the thermal reduction of ceria, which is absent in the simulations, is an endothermic process. The experimental peak and the average heating rates for the power 3800 kW are reported to be 130 K/min and 39 K/min respectively, whereas in the simulations they are about 139 K/min and 45 K/min. The heating rates for power P = 2.8 kW, 3.4 kW and P = 3.4 kW are provided in Table 1. The maximum temperatures obtained and their relative errors in comparison to the experiments are provided in Table 2. From Fig. 3 it can be further noticed that in both the experiments and in the simulations the temperature values have not reached their respective plateaus, but there is a gradual decrease in the heating rates and the temperatures tend towards reaching asymptotic values. It was reported by Furler et al. [2] that the degree of reduction per unit time becomes smaller as the heating rate decreases. The simulations will help in optimizing the duration of the reduction step so that maximum solar-fuel efficiencies ($\eta_{solar\text{-}fuel}$) are attained.

Table 1. Comparison of simulated and experimental peak and average heating rates of ceria RPC

Power input in kW	Peak, average heating rates in K/min (Simulations)	Peak, and average heating rates in K/min (Experiments)
2.8	107, 34	80, 30
3.4	124, 41	110, 35
3.8	139, 45	130, 39

Table 2. Comparison of simulated ceria RPC nominal temperatures to that of experiments

Power input in kW	RPC temperature in K (Simulations)	RPC temperature in K (Experiments)	Relative error in %
0.8	1010	1013	-0.3
2.8	1757	1693	+3.8
3.4	1914	1803	+6.15
3.8	2007	1873	+7.15

Fig. 4 shows the temperature contours within the reactor for the input power 3.8 kW. The maximum RPC temperature is 2592 K and the minimum temperature is 723 K, and this temperature difference happens within 0.02 m of RPC's cylindrical thickness, which results in high temperature gradient and may lead to very high thermal stress in the RPC structure. The thermal stress may be one of the possible reasons behind the structural failure of the porous structure.

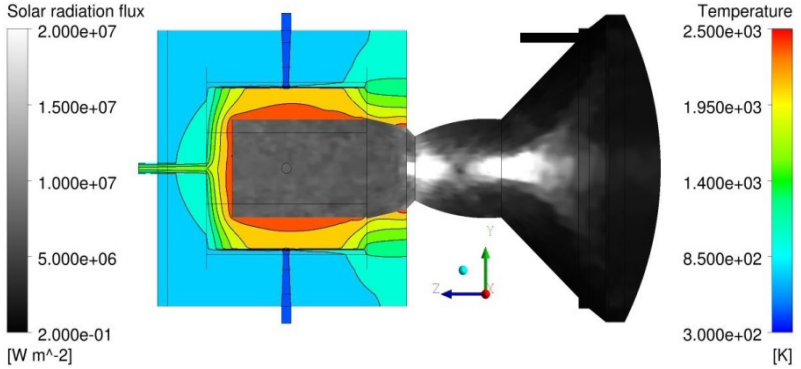

Fig. 4. Cut-plane view of solar flux distribution and temperature contours inside the reactor for power P = 3.8 kW.

The velocity vectors for the fluid flow inside the solar reactor as well as a temperature contour plot are shown in Fig. 5. The fluid entering the reactor through four radial inlet ports have a uniform radial flow across the porous RPC cylinder. Due to convective heat transfer between the solid strut and the fluid, the fluid gets heated up in the porous domain and enters the cavity-receiver with a higher temperature. Though the flow is convectively forced (Ar inflow), its timescale is of the same order as natural convection. Buoyancy plays a role in the movement of hot fluid within the reactor. The hot fluid moves along the top regions of the reactor cavity and imparts a circular flow inside the reactor. This causes the hot fluid to flow into the CPC and towards the window. The mixing of hot fluid with the incoming cooling fluid may impact the cooling of the solar receiver and CPC surfaces. The problems faced in experiments concerning fluid flow are the flow of oxygen over the polished aluminum surfaces during reduction step and the flow of water vapor over the quartz window during the oxidation process. The flow of oxygen over aluminum surfaces at high temperatures oxidizes the aluminum and changes the reflection properties of polished aluminum. The flow of water vapor diffuses the solar flux entering the reactor. Both these effects should be controlled for an effective working of the reactor. With the help of the simulation results, changes can be made to the present reactor construction, which may help in avoiding the above mentioned consequences due to the flow of reacting fluid onto the receiver section. The effect of buoyancy on the temperature of ceria RPC is negligible.

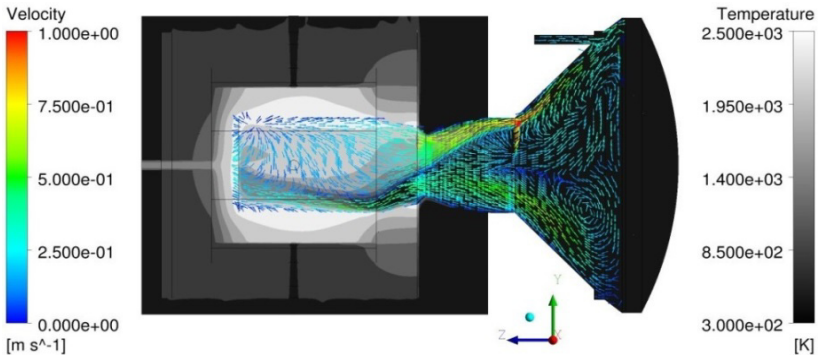

Fig. 5. Cut-plane view showing the velocity vectors of the fluid flow inside the reactor for power input P = 3.8 kW.

5. Conclusion

The solar flux distribution and the direction of radiative intensity inside the fluid regions of the reactor were simulated using the Monte-Carlo radiative model. Rosseland diffusion approximation model was used to simulate the radiative flux in the solid sections of the porous region. Darcy's pressure drop model was used to account for the increase in pressure drop for the fluid flow in the porous sections of the reactor. Two separate energy equations were solved to simulate the heat transport in the solid and fluid regions of the porous reactor. The temperature profiles of the simulations are compared to the experiments, and the results match the experiments with minimum relative errors. Simulation are used to verify the numerical methods and the above mentioned models to compute the heat transfer and fluid transport in a solar chemical reactor.

Acknowledgements

This work has been financially supported by the European Commission under Contract No. 285098 – Project SOLAR-JET. We gratefully appreciate and thank Dr. Philipp Furler (Dept. Mechanical and process engineering, ETH Zurich) for providing us the experimental data and for the fruitful discussions.

References

[1] Chueh WC, Falter C, Abbott M, Scipio D, Furler P, Haile S M, Steinfeld A. High-Flux Solar-Driven Thermochemical Dissociation of CO_2 and H_2O using Nonstoichiometric Ceria. Sceince 2010;330:1797-1801.
[2] Furler P, Scheffe J, Gorbar M, Moes L, Vogt U, Steinfeld A. Solar Thermochemical CO_2 Splitting Utilizing a Reticulated Porous Ceria Redox System. Energy & Fuels 2012;26:7051-7059.
[3] Abanades S, Villafan-Vidales HI. CO_2 and H_2O conversion to solar fuels via two-step solar thermochemical looping using iron oxide redox pair. Chem Eng J 2011;175:368–375.
[4] Loutzenhiser PG, Steinfeld A. Solar syngas production from CO_2 and H_2O in a two-step thermochemical cycle via Zn/ZnO redox reactions: thermodynamic cycle analysis. Int J Hydrogen Energy 2011;36:12141-47.
[5] Lorentzou S, Karagiannakis G, Pagkoura C, Zygogianni A, Konstandopoulos AG. Thermochemical CO_2 and CO_2/H_2O splitting over $NiFe_2O_4$ for solar fuels synthesis. Energy Procedia 2014; 49 :1999 – 2008
[6] Chueh WC, Haile SM. A thermochemical study of ceria: exploiting an old material for new modes of energy conversion and CO_2 mitigation. Philos. Trans. R. Soc. 2010;368:3269-3294.
[7] Furler P, Scheffe J, Steinfeld A. Syngas production by simultaneous splitting of H_2O and CO_2 via ceria redox reactions in a high-temperature solar reactor. Energy & Environmental Science 2012;5:6098-6103.
[8] Steinfeld A, Solar thermochemical production of hydrogen—a review. Solar Energy 2005;78: 603–615.
[9] Steinfeld A, Schubnell M. Optimum Aperture Size and Operating Temperature of a Solar Cavity-Receiver. Solar Energy 1993;50:19-25.
[10] Bear J. Dynamics of Fluid in Porous Media. 1972. American Elsevier Publishing Company. New York:American Elsevier Publishing Company;1972.
[11] Whitaker S. Theory and Application of Transport in Porous Media: The Method of Volume Averaging. London:Kluwer Academic;1999.
[12] Nield DA, Bejan A. Convection in Porous Media. 3rd ed. New York:Springer;2006.
[13] Haussener S. Tomography-based determination of effective heat and mass transport properties of complex multi-phase media. Diss., Eidgenössische Technische Hochschule ETH Zürich 2010.
[14] Howell JR, Siegel R. Thermal Radiation Heat Transfer. 3rd ed. Washington:Taylor and Francis;1992.
[15] Kaviany M. Principles of Heat Transfer in Porous Media. 2nd ed. New York:Springer;1995.
[16] ANSYS CFX Reference Guide. ANSYS CFX Release 15.0;2013.
[17] Howell JR. Radiative transfer in porous media. In: Vafai K(ed). Handbook of Porous Media. New York: Marcel Dekker;2000.p. 663–698.
[18] Modest MF. Radiative heat transfer. 3rd ed. San Diego:Elsevier Science;2013.
[19] Touloukian YS. Thermal radiative properties: nonmetallic solids. New York:IFI/Plenum;1972.
[20] Kolb GJ, Diver RB. Screening analysis of solar themochemical hydrogen concepts. 2008; SANDIA REPORT, SAND2008-1900.